Reversal of the Circular Dichroism in Angle-Resolved Photoemission from Bi_2Te_3

M. R. Scholz,[1,*] J. Sánchez-Barriga,[1] J. Braun,[2] D. Marchenko,[1] A. Varykhalov,[1] M. Lindroos,[3] Yung Jui Wang,[4] Hsin Lin,[4] A. Bansil,[4] J. Minár,[2] H. Ebert,[2] A. Volykhov,[5] L. V. Yashina,[5] and O. Rader[1]

[1]*Helmholtz-Zentrum Berlin für Materialien und Energie, Elektronenspeicherring BESSY II, Albert-Einstein-Strasse 15, 12489 Berlin, Germany*

[2]*Department Chemie, Ludwig-Maximilians-Universität München, Butenandtstrasse 5-13, 81377 München, Germany*

[3]*Institute of Physics, Tampere University of Technology, P.O. Box 692, 33101 Tampere, Finland*

[4]*Physics Department, Northeastern University, Boston, Massachusetts 02115, USA*

[5]*Department of Chemistry, Moscow State University, Leninskie Gory 1/3, 119992 Moscow, Russia*

(Received 4 July 2012; revised manuscript received 9 March 2013; published 22 May 2013)

The helical Dirac fermions at the surface of topological insulators show a strong circular dichroism which has been explained as being due to either the initial-state spin angular momentum, the initial-state orbital angular momentum, or the handedness of the experimental setup. All of these interpretations conflict with our data from Bi_2Te_3 which depend on the photon energy and show several sign changes. Our one-step photoemission calculations coupled to *ab initio* theory confirm the sign change and assign the dichroism to a final-state effect. Instead, the spin polarization of the photoelectrons excited with linearly polarized light remains a reliable probe for the spin in the initial state.

DOI: 10.1103/PhysRevLett.110.216801 PACS numbers: 73.20.At, 79.60.Bm, 71.15.Mb, 75.70.Tj

Topological insulators are characterized by an insulating bulk and a metallic surface. The gap in the bulk bands is due to a band inversion caused by strong spin-orbit interaction [1–7]. Typical examples for which these gaps are rather large are the systems Bi_2Se_3 and Bi_2Te_3. The metallic surface states are protected by time-reversal symmetry [4–7] and display the linear $E(k)$ dispersion of Dirac fermions as demonstrated by angle-resolved photoemission spectroscopy (ARPES) [8,9]. By the same method, the surface states prove robust [10–15]. The peculiar spin topology is of helical type and can also be resolved by ARPES when spin polarimetry is added to the experiment [16].

However, spin-resolved ARPES is a rather demanding detection method since the spin polarimetry reduces the ARPES signal by 2–3 orders of magnitude. On the other hand, there are many interesting subjects that require the measurement of the spin polarization and momentum-dependent spin direction, for example, questions of whether the in-plane spin component remains locked perpendicularly to the momentum in a warped Dirac cone or is in-plane or out-of-plane tilted [16–18], what the maximum value of the polarization is [19–23], and how the spin behaves in the subsurface region [24] and during hybridization with bulk states [25].

It is, therefore, attractive to search for an alternative method of investigation that gives the same information. In photoemission of core levels, the spin resolution is largely complementary to circular dichroism in which the photoemission intensities for excitation with left- and right-circularly polarized radiation, $I_L(E)$ and $I_R(E)$, respectively, are evaluated as a function of binding energy E. The data from both methods can be analyzed straightforwardly with the same atomic model, as the example of spin-split $5p$ core levels of Gd and Tb shows [26,27]. Also in the valence band, a circular dichroism effect in ARPES is present and can be related to the electron spin in ferromagnetic transition metals [28,29].

We have recently observed a strong circular dichroism effect in ARPES from the topological surface state of Bi_2Te_3 [21]. Spin-resolved ARPES from the same system excited by linearly polarized light has been compared to the circular dichroism in ARPES without spin resolution. This showed that the circular dichroism reverses together with the spin texture at the binding energy of the Dirac point [21]. The circular dichroism asymmetry $A = (I_L - I_R)/(I_L + I_R)$ was found to be very large ($> 20\%$ [21]) when compared to measurements from ferromagnets ($\sim 3\%$–5% [28,29]).

For Bi_2Se_3, a strong spin polarization of the topological surface state has been observed by spin-resolved ARPES [18,22,23], and in addition several measurements of the circular dichroism in ARPES have been reported for this system [30–32]. Wang *et al.* conducted circular dichroism measurements at a photon energy of $h\nu = 6$ eV using a pulsed laser source and a time-of-flight detector [30]. The dichroism effect is interpreted assuming transitions into a spin-degenerate continuum of final states and, therefore, is sensitive only to the spin in the initial state of the photoemission process. By measuring one spin component in the surface plane under two different angles and applying symmetry arguments, the two in-plane spin components $\langle S_x \rangle$, $\langle S_y \rangle$ and the perpendicular component $\langle S_z \rangle$ are determined [30]. Another measurement on Bi_2Se_3 at photon energies of 10 and 13 eV led to similar results and a circular dichroism effect of 30% [31(a)]. Park *et al.* concluded that for these photon energies a free-electron final state can be assumed and for left- and right-circularly polarized light final states of different orbital angular

momentum character are reached. The orbital angular momentum was found to be locked to the momentum in a similar way as the spin, and the orbital and spin angular momenta were determined to be antiparallel to each other [31(a)]. Jung *et al.* reached the same conclusion of antiparallel orbital and spin angular momenta for Bi_2Te_3 [31(b)]. Ishida *et al.* compared Cu-doped Bi_2Se_3 to $SrTiO_3$ for which a dichroism effect >60% is observed [32]. The measured circular dichroism of $Cu_xBi_2Se_3$ at $h\nu \sim 7$ eV appears similar to that reported in the other studies but is assigned to a geometrical origin. In the corresponding experimental setup there are two planes perpendicular to the sample surface for which the dichroism disappears [32]. This is, first of all, the detection plane spanned by the incident light and the photoelectron momentum. Furthermore, another plane normal to the surface and perpendicular to the detection plane is identified where the dichroism disappears as well because of the wave function symmetry. This plane is a nodal plane only for circular dichroism of the topological surface state due to a mirror symmetry of its effective Hamiltonian and its two-dimensionality, in contrast to the bulk valence band states. Accordingly, it can be seen as a specific feature reflecting the two-dimensionality [33] of the electronic states [32].

In the present work, we investigate the circular dichroism in ARPES of Bi_2Te_3 for different photon energies and demonstrate that our data question the previous interpretations. It is concluded that current explanations are too simple and a more detailed theoretical treatment is required. Corresponding calculations are conducted and compared to the experiment.

We have grown single crystals of Bi_2Te_3 by the Bridgman method and cleaved them *in situ*. The achieved (111) surfaces are of high quality as concluded from the sharp features in angle-resolved photoemission of the valence band (Fig. 1). Measurements have been carried out in ultrahigh vacuum of 1×10^{-10} mbar at low temperature (30–40 K) with a Scienta R8000 electron analyzer at the UE112-PGM2a beam line of BESSY II with circularly polarized undulator radiation. The geometry of the experiment is shown in Fig. 1.

The bulk electronic structure of Bi_2Te_3 is obtained by performing first-principles calculations within the framework of the density functional theory using the generalized gradient approximation to model exchange-correlation effects [34]. The spin-orbit coupling is included in the self-consistent cycles of the electronic structure calculation.

The angle-resolved photoemission intensity calculations are based on the one-step model [35]. We use a fully relativistic formalism, allowing us to consider in a natural way effects in the photocurrent calculation induced by spin-orbit coupling because the practical calculation is based on the Dirac formalism [36,37]. The spin-orbit coupling enters thus in the calculation of the ground state and again in the photoemission calculation. The photoemission calculation itself is based on multiple-scattering theory, using explicitly the low-energy electron diffraction

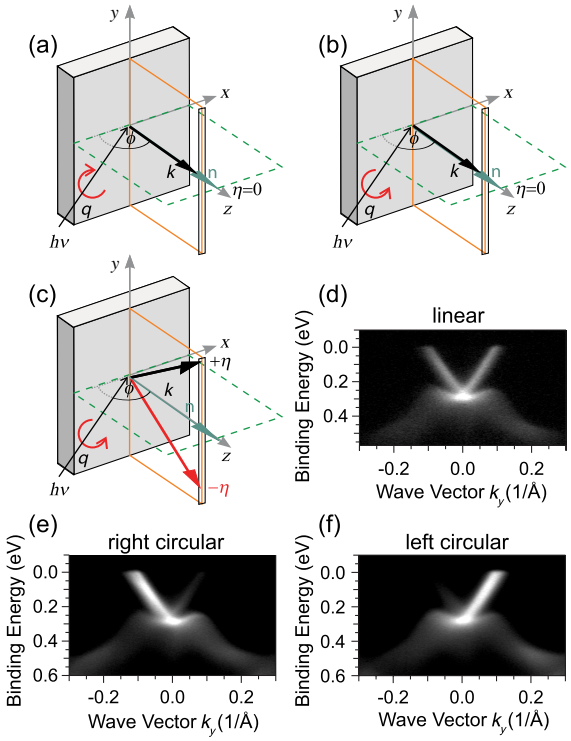

FIG. 1 (color online). (a)–(c) Experimental photoemission geometry and comparison between Bi_2Te_3 data along the $\bar{\Gamma}$-$\bar{K}$ direction excited by (d) linearly and (e) right- and (f) left-circularly polarized light of $h\nu = 55$ eV. The topological surface state is identified by its linear dispersion upwards from the Dirac point around 0.25 eV binding energy, and the dichroism is strongly visible without need for difference spectra.

(LEED) method to calculate the initial and final states for a semi-infinite atomic half-space. In this way, the final state is calculated by the best available single-particle approach as a so-called time-reversed LEED state [38]. In line with this, the initial state is represented by the retarded one-electron Green function for the same semi-infinite half-space. The photoemission calculations include matrix-element effects, multiple scattering effects in the initial and final states, the effect of the photon momentum vector, and the escape depth of the photoelectrons via an imaginary part in the inner potential. These lifetime effects in the final states have been included in our analysis in a phenomenological way using a parametrized complex inner potential $V_o(E) = V_{or}(E) + iV_f(E)$. Herein, the real part serves as a reference energy inside the crystal with respect to the vacuum level. To account for impurity scattering, a small constant imaginary value of $V_i = 0.004$ eV was used for the initial state. A realistic description of the surface potential is given through a Rundgren-Malmström barrier [39] which connects the asymptotic regime $z < z_A$ to the bulk muffin-tin zero V_{or} by a third order polynomial in z, spanning the range $z_A < z < z_E$. In other words, z_A defines the point where the polynomial region starts, whereas z_E defines the point where the surface region ends and the bulk region starts with the first atomic layer. The effective z-dependent surface barrier V is scaled with

respect to the vacuum level $E_{vac} = 0.0$ eV utilizing the value of the work function $\phi = 5.0$ eV. The zero of the z scale lies in the uppermost layer of atoms.

The geometrical origin for a circular dichroism in ARPES, as has been described in detail in Ref. [29], can be understood on the basis of Fig. 1. No dichroism is expected when the geometry is such that a symmetry operation which transforms right- into left-circularly polarized light leaves the momentum vector of the photoelectron $\mathbf{k}$ unaffected. This is shown at the top of Fig. 1. The green plane ($\eta = 0°$, $k_y = 0$, dashed line) is the plane of incidence and is a mirror plane (crystal symmetry provided) transforming the right-circularly polarized light of Fig. 1(a) into the left-circularly polarized light of Fig. 1(b) without affecting $\mathbf{k}$. The green plane constitutes, therefore, a nodal plane meaning zero dichroism for $k_y = 0$. For all other situations a dichroism can occur, for example, in the yellow plane ($k_x = 0$), which is the detector plane. (The detector slit is indicated as a narrow vertical rectangle in Fig. 1.) Reversal of the light polarization changes $\mathbf{k}$ from $+\eta$ to $-\eta$ [Fig. 1(c)], which means opposite sign of the dichroism for emission angles $+\eta$ and $-\eta$ [Fig. 1(d)]. Figures 1(e)–1(g) show separately the photoemission intensity for right- and left-circularly polarized light of Bi_2Te_3. The effect is apparently very large and visible already comparing the intensities I_L and I_R. The corresponding asymmetry A is then shown in a color representation in Figs. 2–4. Figures 2–4 display a white line in their center, $k_y = 0$, that represents the nodal plane mentioned above. As can be seen, not only the topological surface state shows the nodal plane but also the bulk states, a fact which would support the interpretation as a geometrical effect. However, it should be stressed that the additional perpendicular nodal plane discussed in Ref. [32] is identical to the plane in which the data of Figs. 1(e)–1(g) and 2 have been measured. This means that the description suggested by Ishida *et al.* as dichroism due to geometrical effects only is not appropriate for our present case. Moreover, the reversal of the dichroism effect at the binding energy of the Dirac point contradicts the model by Ishida *et al.* because this behavior cannot be explained based on purely geometrical effects.

Figure 2 shows the behavior of the circular dichroism in the experiment at photon energies between 21 and 100 eV. The asymmetry is very large (80% at $h\nu = 55$ eV). (Note that, as a two-dimensional state, the topological surface state has a binding energy independent of the photon energy which may still change slightly within Fig. 2 due to surface doping by residual gas.) In Figs. 2(a)–2(d) we show complete $E(\mathbf{k}_\parallel)$ dispersion relations which are all characterized by a circular dichroism effect that changes sign with binding energy at the Dirac point. Generally, the lower-binding-energy range shows a large dichroism effect. ($\mathbf{k}_\parallel$ is the projection of the electron wave vector on the surface plane.) This range contributes spectral intensity of the topological surface state only while the higher-binding-energy range has to some extent bulklike contributions as well. We see that for each selected photon energy in Figs. 2(a)–2(d) the complete circular dichroism signal has reversed sign, above as well as below the Dirac point. Figure 2(e) shows for $h\nu < 70$ eV the detailed behavior with smaller steps in photon energy. The behavior around 45 eV may indicate additional sign changes [40]. According to the initial-state model for the spin [30], the data in Fig. 2 would mean that the spin of the probed ground state changes during the photon energy scan. This is not possible, not even under the assumption of a layered spin texture, which has been predicted to reverse in the topmost atomic layers [24], because the photocurrent from the topmost layer dominates in the photoemission signal from the topological surface state. A similar problem arises with the initial-state orbital angular momentum model [31] because, again, it is unclear how the probed initial state can depend on the photon energy of the probing radiation.

We have, therefore, performed calculations for the ground state and calculated the photoemission spectra as described briefly above. Figure 3(a) shows the resulting dichroism in ARPES at $h\nu = 27$ eV using the same representation as for the experimental data. As can be seen, the angle- and the binding-energy dependences are very similar to the experiment in Fig. 2. For investigating the origin of the dichroism effect further, our photoemission calculations allow us to vary the spin-orbit-coupling strength. The idea behind this is that the decoupling of spin and orbital moment will reduce the effect that the spin polarization can have on the circular dichroism. A reduced spin-orbit coupling can be simulated simply by an increased speed of light c_0. Before applying this in Fig. 3, we tested the use of $1.09c_0$ and $1.24c_0$ on the spin-orbit splitting of W metal between Γ_{7+} and Γ_{8+} states and obtained 90% and 75%, respectively, of the original splitting. This effect is not too far from the expected scaling with $1/c_0^2$ in the atom. The first impact that one notes in

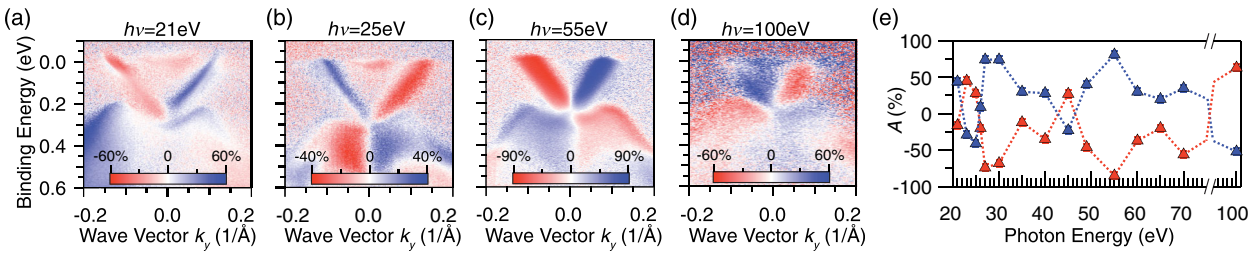

FIG. 2 (color online). Change of the circular dichroism effect with photon energy. (a)–(d) The upper row shows three reversals of the sign between photon energies of 21 and 100 eV. (e) Plot of the dichroism asymmetry A evaluated 100 meV above the Dirac point versus photon energy. The dichroism asymmetry is large (80% at $h\nu = 55$ eV).

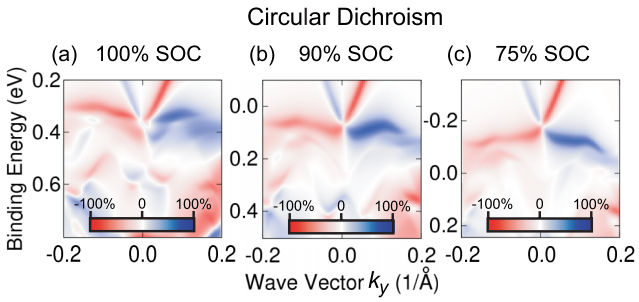

FIG. 3 (color online). Calculations for a reduced spin-orbit interaction for the example of $h\nu = 27$ eV. The spin-orbit coupling (SOC) is reduced from (a) 100% (c_0) to (b) 90% ($1.09c_0$) and (c) 75% ($1.24c_0$). This modifies the inverted bulk band gap and moves the topological surface state in energy. The circular dichroism remains very similar, indicating a minor role of the electron spin polarization for the circular dichroism. The overall change in binding energy is a side effect and not relevant here.

Fig. 3 is the change in the binding energy of the Dirac point. This is due to the effect of the spin-orbit coupling on the bulk band inversion. It should be stressed that if the spin-orbit coupling would be reduced further, the band inversion and with it also the topological surface state would disappear. Figures 3(b) and 3(c) show that the changes of the circular dichroism of the topological surface state are rather small when the spin-orbit coupling is reduced. This suggests that the contribution of the spin to the circular dichroism is a minor one, and we will return to this question further below in connection with the photon-energy dependence.

One-step photoemission intensities in general are based on ground state electronic structure calculations and, as a consequence, the energetics of the final states obtained for higher photon energies often deviates from the experimental situation depending on the excitation energy. In this sense, our calculations have qualitative character and do not, e.g., reproduce the position of the experimental sign change between 21 and 25 eV photon energy. However, Fig. 4 shows that between 25 and 50 eV the sign has clearly reversed in the calculation. This is an important confirmation of the experimental results of Fig. 2 demonstrating that the sign change is reproduced by our photoemission theory and can be ascribed to the final states.

We have previously investigated the L-gap surface state of Cu(111) by one-step photoemission calculations for a wide photon energy range from 21 to 70 eV and compared to ARPES experiments [41]. In that case, the dichroism asymmetry depends on the photon energy as well. An analysis of the final states confirmed that the dichroism effect is strong where a d-type final state is reached in agreement with the expectations from selection rules for the orbital angular momentum [41]. This mechanism has been discussed later on in a very similar context in an ARPES study on Cu(111) and Au(111) [42]. The same mechanism underlies the present results which also involve transitions from p-type initial states to d-type final states. When the present calculation is modified to exclude transitions into d-type final states, the sign change between 25 and 50 eV photon energy disappears [40]. The final states

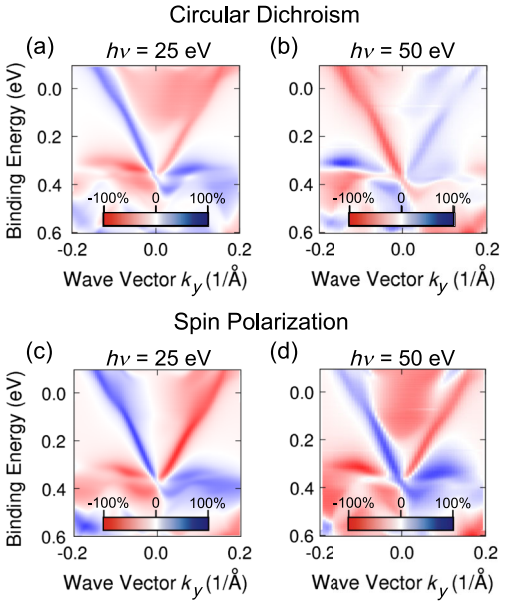

FIG. 4 (color online). Results from the one-step photoemission calculation. Top: Calculated circular dichroism changes sign between photon energies of (a) 25 eV and (b) 50 eV. Bottom: For the same system but linearly polarized light. The calculated spin polarization P of the photoemission from the topological surface state is unaffected by the photon energy. It reaches $P \sim 80\%$ at 25 eV in (c) and 75% at 50 eV in (d).

are, however, more difficult to analyze than in fcc Cu due to frequent backfolding because of the small size of the bulk Brillouin zone along z (perpendicular to the surface). An analysis of the initial state identifies the topological surface state as being due to all three p orbitals, and this is the reason for the stronger dependence on the final states concerning the sign changes as compared to the p_z-type surface state of Cu(111). The spin-orbit coupling is much weaker in Cu when compared to the present system Bi_2Te_3. The fact that spin-orbit coupling is not a precondition for a strong circular dichroism in ARPES has been demonstrated also early on: In graphite, transitions from the π band into d final states lead to dichroism asymmetries of up to 60% at a negligibly small spin-orbit coupling [43]. It should be stressed that spin-orbit interaction also induces a $\mathbf{k}$-dependent spin polarization of the initial states, simply due to the presence of the surface [44]. This effect, which is quantitatively considered in our analysis, has to be accounted for to fully understand the experimental data.

Figure 4 also allows us to inspect the potential of spin-resolved photoemission and its dependence on the final states. The bottom row of Fig. 4 shows the calculated spin polarization $P = (I^{\uparrow} - I^{\downarrow})/(I^{\uparrow} + I^{\downarrow})$ of the photoelectrons as a function of the photon energy for linearly polarized light. The sign of the spin polarization remains constant and also its value is practically the same ($P = 80\%$ at 25 eV and 75% at 50 eV when evaluated 100 meV above the Dirac energy). This means that spin-resolved photoemission is much less affected by final-state effects than the circular dichroism and, therefore, can be used to deduce the electron spin in the initial state rather directly. This has

to do with the fact that the circular dichroism is the difference of two signals and by itself very sensitive while for the initial-state spin the phase space for excitation by linearly polarized light is less restricted.

In summary, we have investigated the dependence of circular dichroism in ARPES from Bi_2Te_3 on the photon energy. Even for final-state energies that are 10 times higher than those considered free-electron-like, we observe a sensitive dependence on the photon energy and a reversal of the sign. The various proposed initial-state models favoring the spin or the orbital angular momentum cannot be applied, and the same holds for pure geometric models. The circular dichroism in ARPES has clearly been identified as a final-state effect experimentally with confirmation by the results of one-step photoemission calculations. The spin polarization of the photoelectrons excited with linearly polarized light is not affected.

O. R. thanks G. Bihlmayer for helpful discussions. Financial support from the Deutsche Forschungsgemeinschaft (Grants No. EB-154/18, No. EB-154/23, and No. SPP 1666) and the Bundesministerium fur Bildung und Forschung (Grant No. 05K10WMA) is gratefully acknowledged. The work at Northeastern University is supported by the US Department of Energy, Office of Science, Basic Energy Sciences Contract No. DE-FG02-07ER46352, and benefited from Northeastern University's Advanced Scientific Computation Center (ASCC), theory support at the Advanced Light Source, Berkeley and the allocation of time at the NERSC supercomputing center through DOE Grant No. DE-AC02-05CH11231.

Note added.—Recent one-step photoemission calculations [45], which do not support the argumentation by Jung *et al.* [31], conclude that the spin texture can be measured by circular dichroism, in particular the out-of-plane component [45]. The dependence on the photon energy has not been studied.

*Present address: Physikalisches Institut, Universität Würzburg, Am Hubland, 97074 Würzburg, Germany.

[1] C. L. Kane and E. J. Mele, Phys. Rev. Lett. **95**, 146802 (2005); **95**, 226801 (2005).
[2] L. Fu and C. L. Kane, Phys. Rev. B **76**, 045302 (2007).
[3] B. A. Bernevig and S. C. Zhang, Phys. Rev. Lett. **96**, 106802 (2006).
[4] L. Fu, C. L. Kane, and E. J. Mele, Phys. Rev. Lett. **98**, 106803 (2007).
[5] J. E. Moore and L. Balents, Phys. Rev. B **75**, 121306 (2007).
[6] R. Roy, Phys. Rev. B **79**, 195322 (2009).
[7] S. Murakami, New J. Phys. **9**, 356 (2007).
[8] Y. Xia *et al.*, Nat. Phys. **5**, 398 (2009).
[9] Y. L. Chen *et al.*, Science **325**, 178 (2009).
[10] L. Plucinski, G. Mussler, J. Krumrain, A. Herdt, S. Suga, D. Grützmacher, and C. M. Schneider, Appl. Phys. Lett. **98**, 222503 (2011).
[11] P. D. C. King *et al.*, Phys. Rev. Lett. **107**, 096802 (2011).
[12] H. M. Benia, C. Lin, K. Kern, and C. R. Ast, Phys. Rev. Lett. **107**, 177602 (2011).
[13] T. Hirahara, G. Bihlmayer, Y. Sakamoto, M. Yamada, H. Miyazaki, S.-I. Kimura, S. Blügel, and S. Hasegawa, Phys. Rev. Lett. **107**, 166801 (2011).
[14] T. Valla, Z.-H. Pan, D. Gardner, Y. S. Lee, and S. Chu, Phys. Rev. Lett. **108**, 117601 (2012).
[15] M. R. Scholz, J. Sánchez-Barriga, D. Marchenko, A. Varykhalov, A. Volykhov, L. V. Yashina, and O. Rader, Phys. Rev. Lett. **108**, 256810 (2012).
[16] J. H. Dil, J. Phys. Condens. Matter **21**, 403001 (2009).
[17] L. Fu, Phys. Rev. Lett. **103**, 266801 (2009).
[18] S. Souma, K. Kosaka, T. Sato, M. Komatsu, A. Takayama, T. Takahashi, M. Kriener, K. Segawa, and Y. Ando, Phys. Rev. Lett. **106**, 216803 (2011).
[19] D. Hsieh *et al.*, Nature (London) **460**, 1101 (2009).
[20] O. V. Yazyev, J. E. Moore, and S. G. Louie, Phys. Rev. Lett. **105**, 266806 (2010).
[21] M. R. Scholz, J. Sánchez-Barriga, D. Marchenko, A. Varykhalov, A. Volykhov, L. V. Yashina, and O. Rader, arXiv:1108.1053v2.
[22] Z.-H. Pan, E. Vescovo, A. V. Fedorov, D. Gardner, Y. S. Lee, S. Chu, G. D. Gu, and T. Valla, Phys. Rev. Lett. **106**, 257004 (2011).
[23] C. Jozwiak *et al.*, Phys. Rev. B **84**, 165113 (2011).
[24] J. Henk, A. Ernst, S. V. Eremeev, E. V. Chulkov, I. V. Maznichenko, and I. Mertig, Phys. Rev. Lett. **108**, 206801 (2012).
[25] S. V. Eremeev *et al.*, Nat. Commun. **3**, 635 (2012).
[26] G. van der Laan, E. Arenholz, E. Navas, Z. Hu, E. Mentz, A. Bauer, and G. Kaindl, Phys. Rev. B **56**, 3244 (1997).
[27] E. Vescovo, O. Rader, G. van der Laan, and C. Carbone, Phys. Rev. B **56**, R11403 (1997).
[28] J. Bansmann, M. Getzlaff, C. Westphal, F. Fegel, and G. Schönhense, Surf. Sci. **269–270**, 622 (1992).
[29] W. Kuch and C. M. Schneider, Rep. Prog. Phys. **64**, 147 (2001).
[30] Y. H. Wang, D. Hsieh, D. Pilon, L. Fu, D. R. Gardner, Y. S. Lee, and N. Gedik, Phys. Rev. Lett. **107**, 207602 (2011).
[31] (a) S. R. Park *et al.*, Phys. Rev. Lett. **108**, 046805 (2012). (b) W. Jung *et al.*, Phys. Rev. B **84**, 245435 (2011).
[32] Y. Ishida *et al.*, Phys. Rev. Lett. **107**, 077601 (2011).
[33] V. B. Zabolotnyy *et al.*, Phys. Rev. B **76**, 024502 (2007).
[34] M. Lindroos, S. Sahrakorpi, and A. Bansil, Phys. Rev. B **65**, 054514 (2002).
[35] J. F. L. Hopkinson, J. B. Pendry, and D. J. Titterington, Comput. Phys. Commun. **19**, 69 (1980).
[36] J. Braun, Rep. Prog. Phys. **59**, 1267 (1996).
[37] H. Ebert, J. Minár, J. Braun, and S. Mankovskyy, J. Electron Spectrosc. Relat. Phenom. **184**, 91 (2011).
[38] A. X. Gray *et al.*, Nat. Mater. **10**, 759 (2011).
[39] G. Malmström and J. Rundgren, Comput. Phys. Commun. **19**, 263 (1980).
[40] See Supplemental Material at http://link.aps.org/supplemental/10.1103/PhysRevLett.110.216801 for more details.
[41] M. Mulazzi, G. Rossi, J. Braun, J. Minár, H. Ebert, G. Panaccione, I. Vobornik, and J. Fujii, Phys. Rev. B **79**, 165421 (2009).
[42] B. Kim *et al.*, Phys. Rev. B **85**, 195402 (2012).
[43] G. Schönhense, C. Westphal, J. Bansmann, and M. Getzlaff, Europhys. Lett. **17**, 727 (1992).
[44] U. Heinzmann and J. H. Dil, J. Phys. Condens. Matter **24**, 173001 (2012).
[45] H. Mirhosseini and J. Henk, Phys. Rev. Lett. **109**, 036803 (2012).